



Implementation of a high resolution, high-contrast magnetic resonance imaging protocol with extended delayed phases for peritoneal mesothelioma

Milica Medved^{1^}, Hunter D. D. Witmer², Ankit Dhiman², Yaniv Berger^{3,4}, Scott K. Sherman⁵, Enal S. Hindi², Samuel G. Armato III¹, Ingrid S. Reiser¹, Aytekin Oto¹, Roger M. Engelmann¹, Hedy L. Kindler⁶, Nisa C. Oren¹, Carla B. Harmath¹, Kiran K. Turaga²

¹Department of Radiology, the University of Chicago, Chicago, IL, USA; ²Department of Surgery, Yale School of Medicine, New Haven, CT, USA; ³Department of Surgery B, Chaim Sheba Medical Center, Ramat Gan, Israel; ⁴Faculty of Medicine, Tel Aviv University, Tel Aviv, Israel; ⁵Division of Surgical Oncology and Endocrine Surgery, Department of Surgery, University of Iowa, Iowa City, IA, USA; ⁶Department of Medicine, the University of Chicago Medicine, Chicago, IL, USA

Contributions: (I) Conception and design: M Medved, HDD Witmer, A Dhiman, SG Armato 3rd, IS Reiser, A Oto, RM Engelmann, CB Harmath, KK Turaga; (II) Administrative support: ES Hindi; (III) Provision of study materials or patients: HDD Witmer, A Dhiman, Y Berger, SK Sherman, HL Kindler, KK Turaga; (IV) Collection and assembly of data: M Medved, RM Engelmann; (V) Data analysis and interpretation: M Medved, HDD Witmer, A Dhiman, Y Berger, SG Armato 3rd, A Oto, RM Engelmann, NC Oren, CB Harmath, KK Turaga; (VI) Manuscript writing: All authors; (VII) Final approval of manuscript: All authors.

Correspondence to: Kiran K. Turaga, MD, MPH. Department of Surgery, Yale School of Medicine, 310 Cedar Street FMB 130J, New Haven, CT 06520, USA. Email: kiran.turaga@yale.edu.

Background: Imaging of peritoneal malignancies using conventional cross-sectional imaging is challenging, but accurate assessment of peritoneal disease burden could guide better selection for definitive surgery. Here we demonstrate feasibility of high-resolution, high-contrast magnetic resonance imaging (MRI) of peritoneal mesothelioma and explore optimal timing for delayed post-contrast imaging.

Methods: Prospective data from inpatients with malignant peritoneal mesothelioma (MPM), imaged with a novel MRI protocol, were analyzed. The new sequences augmenting the clinical protocol were (I) pre-contrast coronal high-resolution T2-weighted single-shot fast spin echo (COR hr T2w SSH FSE) of abdomen and pelvis; and (II) post-contrast coronal high-resolution three-dimensional (3D) T1-weighted modified Dixon (COR hr T1w mDIXON) of abdomen, acquired at five delay times, up to 20 min after administration of a double dose of contrast agent. Quantitative analysis of contrast enhancement was performed using linear regression applied to normalized signal in lesion regions of interest (ROIs). Qualitative analysis was performed by three blinded radiologists.

Results: MRI exams from 14 participants (age: mean \pm standard deviation, 60 \pm 12 years; 71% male) were analyzed. The rate of lesion contrast enhancement was strongly correlated with tumor grade (cumulative nuclear score) ($r=-0.65$, $P<0.02$), with ‘early’ delayed phase (12 min post-contrast) and ‘late’ delayed phase (19 min post-contrast) performing better for higher grade and lower grade tumors, respectively, in agreement with qualitative scoring of image contrast.

Conclusions: High-resolution, high-contrast MRI with extended post-contrast imaging is a viable modality for imaging peritoneal mesothelioma. Multiple, extended (up to 20 min post-contrast) delayed phases are necessary for optimal imaging of peritoneal mesothelioma, depending on the grade of disease.

[^] ORCID: 0000-0003-2945-5511.

Keywords: Peritoneal surface malignancy; malignant mesothelioma; magnetic resonance imaging (MRI); gadolinium (Gd)

Submitted Jan 05, 2023. Accepted for publication Dec 18, 2023. Published online Mar 06, 2024.

doi: 10.21037/qims-23-13

View this article at: <https://dx.doi.org/10.21037/qims-23-13>

Introduction

Radiographic assessment of peritoneal malignancies is challenging due to frequently small tumor size or thickness, similar density and signal intensity to adjacent structures, variable distribution of disease, and unpredictable contrast enhancement. Malignant peritoneal mesothelioma (MPM) is one such malignancy necessitating careful diagnostic assessment prior to attempting definitive surgical resection (1-4). Unfortunately, modern imaging modalities have suboptimal diagnostic ability for determining unresectable disease. Underestimation of disease burden by axial imaging is a known limitation and results in a reliance on invasive diagnostic laparoscopy for accurate staging (5-7). Imprecise clinical staging can lead to futile attempts at surgical resection and a delay in guiding patients with unresectable disease to more appropriate or palliative treatment (7,8). Better diagnostic certainty would reduce the management burden on patients and improve surgeon and patient confidence in the treatment plan (4,9).

Current Peritoneal Surface Oncology Group International (PSOGI) guidelines recommend computed tomography (CT) as the preferred pre-operative diagnostic modality despite scarce supporting data (10); however, these guidelines and the literature also suggest that magnetic resonance imaging (MRI) could be used for pre-operative evaluation despite unanswered questions regarding its accuracy for detection and characterization of disease burden (3,5,8,11). Prospective assessment of peritoneal-specific MRI, especially for mesothelioma, has not been implemented due to the low resolution of MRI axial imaging and technical challenges involved. However, while a CT scan provides better slice thickness and spatial resolution than conventional MRI, MRI offers significantly better tissue discrimination of disease and the ability to optimize for contrast enhancement, without ionizing radiation (5,10-12). In addition, the optimal timing of post-contrast imaging for highlighting and characterizing peritoneal lesions remains unknown and is more safely studied with a non-ionizing modality.

In this study, we describe novel radiological advances

in imaging the peritoneum noted during the course of a phase II clinical trial (NCT #03867578) examining the role of high resolution, high contrast MRI in imaging the peritoneal cavity prior to surgical resection in patients with peritoneal mesothelioma, and examine the time dependence of lesion signal intensity after magnetic resonance contrast administration.

Methods

Study subjects & recruitment

Patients presenting to a multi-disciplinary mesothelioma clinic at the University of Chicago were screened for inclusion in this phase II prospective clinical trial (NCT #03867578) between February of 2019 and August of 2020. Consecutive recruitment from a homogeneous population was used to minimize potential bias. This study was conducted in accordance with the Declaration of Helsinki (as revised in 2013). The study was approved by the Institutional Review Board of the Biological Sciences Division of the University of Chicago (No. IRB18-1011) and informed consent was taken from all individual participants. The inclusion criteria included age ≥ 18 years, biopsy-proven MPM, cytoreductive surgery planned within 60 days, ability to safely undergo and tolerate contrast-enhanced CT, contrast-enhanced MRI, and ultrasound scans, and ability and willingness to use appropriate contraceptive methods before imaging and for a period of 365 days thereafter. The exclusion criteria included pregnancy or breastfeeding and counter-indications for undergoing imaging exams.

Enrolled participants underwent a research MRI using our novel protocol 1–5 weeks prior to the surgical assessment of disease via a diagnostic laparoscopy or definitive cytoreductive surgery. Conventional axial CT imaging was obtained per standard of care.

Participants' clinical and demographic data were recorded, including age, sex, intraoperative assessment of disease burden [peritoneal cancer index (PCI) score], history of cardiac disease, histological subtype, pathology results

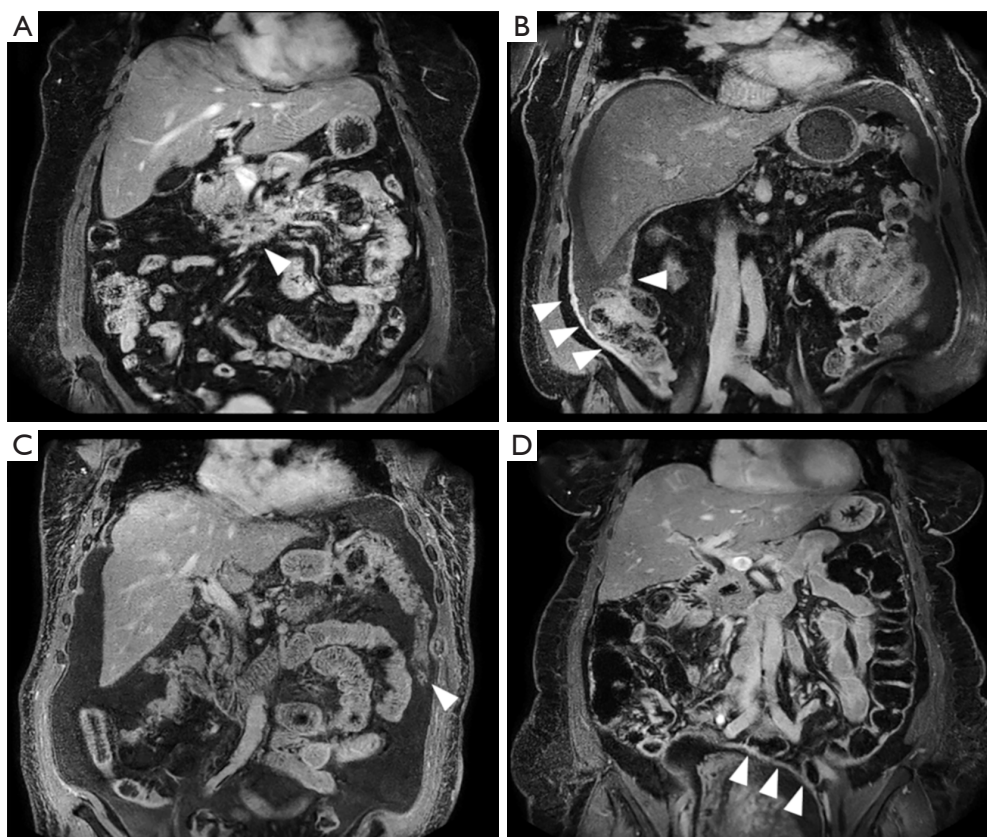


Figure 1 Examples of post-contrast COR hr T1w mDIXON (water-only) images acquired through the abdomen of four subjects, at delay times of 12.5–14 min are shown (A–D). Anatomical structures are shown in sharp detail with adequate SNR. Lesion enhancement is evident, with some of the enhanced lesions indicated with arrowheads. COR hr T1w mDIXON, coronal high-resolution 3D T1-weighted modified Dixon; 3D, three-dimensional; SNR, signal-to-noise ratio.

[nuclear grade and cumulative nuclear score (nuclear atypia and mitotic count)] (13), and receipt of prior neoadjuvant therapy and prior cytoreductive surgery. Pathology results were reported post-cytoreductive surgery as the highest grade/score observed.

MRI protocol

Participants were scanned on a 3T dStream Ingenia MRI scanner (Philips Healthcare, Andover, MA, USA), using the anterior surface coil and posterior elements built into the scanner bed. The new sequences introduced to enhance the standard clinical abdominal MRI protocol were (I) pre-contrast coronal high-resolution T2-weighted single-shot fast spin echo (COR hr T2w SSH FSE; spatial resolution $0.80 \times 0.80 \times 3.00 \text{ mm}^3$) of abdomen and pelvis; and (II) post-contrast coronal high-resolution three-dimensional (3D)

T1-weighted modified Dixon (COR hr T1w mDIXON; spatial resolution $1.20 \times 1.16 \times 3.00 \text{ mm}^3$) of abdomen and upper pelvis, with anterior/posterior coverage of 23 cm, and acquired at multiple delay times, up to 20 min after contrast administration. Additionally, a double dose (0.2 mmol/kg) of gadoterate meglumine (Dotarem; Guerbet LLC, Princeton, NJ, USA) was administered to increase contrast. The choice of contrast agent was guided by established safety profiles regarding stability *in vitro* and *in vivo* (14–19). Specific imaging parameters for the full MRI protocol are listed in [Table S1](#), that can be found online. Diffusion-weighted imaging (DWI) was not included, as it was not possible to achieve spatial resolutions necessary for identification of small, flat or linear lesions. *Figure 1* shows examples of delayed post-contrast COR hr T1w mDIXON images in four subjects. Anatomical structures are shown in sharp detail with adequate SNR and lesion enhancement is evident.

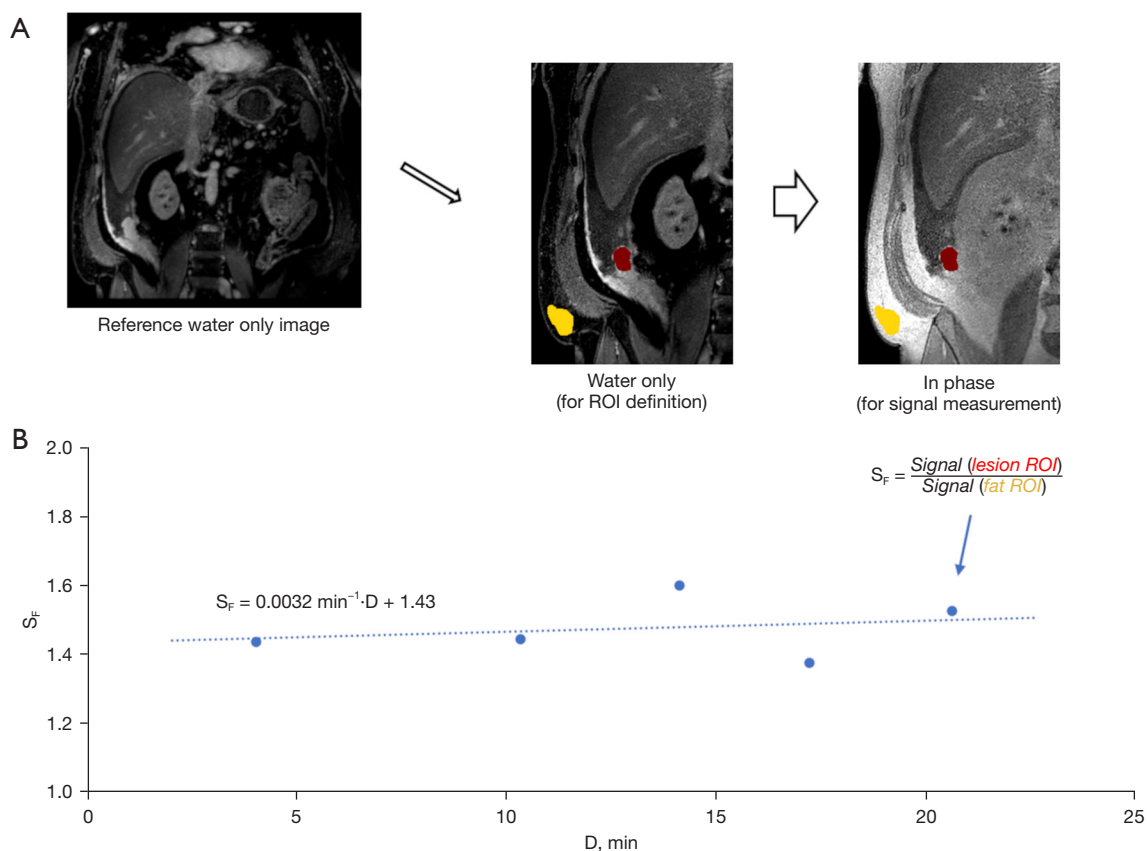


Figure 2 Calculation of slope A_F is illustrated. (A) A whole-field COR hr T1w mDIXON (water-only) image is shown for reference. An enlarged sub-region of water-only and in-phase mDIXON images is also shown. The lesion (red) and subcutaneous fat (yellow) ROIs are outlined on the water only image, and the signal intensities are measured on the in-phase image. (B) The ratio of the lesion ROI and subcutaneous fat ROI signal intensities yields S_F at each delay time D . Using Eq. [1], S_F is fit as a function of D . In this example, $A_F = 3.2 \times 10^{-3} \cdot \text{min}^{-1}$. ROI, region of interest; COR hr T1w mDIXON, coronal high-resolution 3D T1-weighted modified Dixon; 3D, three-dimensional.

Region of interest (ROI) definition

The COR hr T1w mDIXON (in-phase) images were loaded into custom-made software for ROI delineation. An experienced abdominal radiologist (C.B.H.) selected freehand-outlined ROIs in the lateral abdominal subcutaneous fat tissue, as well as several lesion ROIs, for each subject on the first post-contrast sequence. The ROIs were propagated and manually adjusted as necessary to match across several additional post-contrast COR hr T1w mDIXON images. The same radiologist classified selected lesions as either linear or mass type.

Quantitative image analysis

Image signal was averaged over each ROI and lesion averages

were normalized to fat ROI average signal. Uptake of contrast agent in fat tissue was assumed to be minimal and therefore fat ROI signal could provide adequate normalization to account for variations in hardware gain between post-contrast COR hr T1w mDIXON sequences within each exam. Lesion ROI signal normalized to fat (S_F) was modeled with a linear function over the 4–20 min post-contrast delay interval to determine the slope A_F in units of min^{-1} [Eq. [1]]:

$$S_F(i) = A_F \cdot D_i + \text{offset} \quad [1]$$

where $S_F(i)$ represents the normalized lesion signal at i -th post-contrast timepoint, D_i represents the delay time of the i -th post-contrast sequence (approximately 4, 7, 13, 16, and 20 min), and offset is the y-axis intercept not used in this study. This method is illustrated in *Figure 2*. Positive

values of A_F indicated continuous increase in normalized signal due to contrast agent uptake in the lesions, while negative values of A_F indicated contrast agent washout and decreasing normalized signal over the 4–20 min delay interval.

A_F values were used in per-lesion analysis. For per-subject analysis, averages \tilde{A}_F for all lesions outlined in a single subject were calculated and correlated with clinical variables.

Qualitative image analysis

Three abdominal radiologists (A.O., N.C.O., C.B.H.) with 10–25 years of experience independently reviewed post-contrast COR hr T1w mDIXON (water only) images acquired at (mean \pm standard deviation) 12.1 \pm 1.3 min ('early') and 19.1 \pm 1.5 min ('late') delay after contrast administration. Only two post-contrast time points were compared, to reduce the complexity of the evaluation. Survey responses were collected on Research Electronic Data Capture (REDCap) (20,21). The radiologists were asked to state their preference for visualization of the peritoneum and potential peritoneal disease, specifically in the pelvis and the right diaphragm. The radiologists were blinded to post-contrast timing of MRI sequences.

Statistical analysis

The intra- and inter-patient variability was assessed using mixed effects regression with patients as random effects. The Wilcoxon signed rank test was used to evaluate whether the mean of all lesion slopes A_F differed from zero. The Wilcoxon rank-sum test was used to evaluate whether the mean of slopes A_F differed between mass versus linear type lesions. The paired test for proportions was used to compare proportions of lesions with positive slopes between mass versus linear type lesions. The threshold for significance was set to $P=0.05$.

Spearman's coefficient of correlation was used to characterize the correlation of \tilde{A}_F with age, pathology nuclear grade, and cumulative nuclear score. Nuclear grade and cumulative nuclear score are highly correlated and were not considered as independent measurements; thus, correcting for multiple comparisons yielded the significance threshold of $0.05/2=0.025$. The Wilcoxon rank-sum test was used to compare the \tilde{A}_F between groups with or

without presence of cardiac disease, prior cytoreductive surgery, and prior chemotherapy, with correction for multiple comparisons yielding the significance threshold of $0.05/3=0.017$.

Spearman's coefficient of correlation was used to characterize the correlation of reader preference for visualization of the peritoneum and potential peritoneal disease with cumulative nuclear score, using the significance threshold of $P=0.05$.

Results

Study and clinical characteristics

Sixteen scans were performed on 14 subjects {age: median [range], 60 [26–74] years}. Although two participants completed scans before and after chemotherapy, only one pre-chemotherapy scan per subject was included in the analysis. One of the participants' scans was excluded from comparison of early versus late delayed phase images because not all five extended-delay post-contrast sequences were performed, but was still included in the quantitative analysis. For one participant who had biphasic disease, pathology grade and cumulative nuclear score were not available.

Median PCI score (quantitative measure of burden of peritoneal disease scored in 13 zones with a score of 0–3 in each zone) was 38 (range, 11–39). Clinical and pathologic characteristics are summarized in *Table 1* (22). Thirteen subjects had epithelioid mesothelioma and grade of the tumor was captured using previously described methods (13).

Quantitative image analysis and correlation to clinical variables

The mean number of outlined lesion ROIs, per subject, was 3.7 [range, 2–6; total 52 lesions (38 mass, 14 linear type)]. Data from two representative lesions from two different subjects are shown in *Figure 3*, illustrating both a positive value for A_F {Eq. [1]}, indicating continuous contrast uptake, and a negative value, indicating contrast agent washout. *Figure 4* illustrates the frequently observed increase in lesion contrast over the examined post-contrast delay times.

In per-lesion analysis, the mean of slopes A_F was $(-3.0\pm 14)\times 10^{-3}\cdot\text{min}^{-1}$ (mean \pm standard deviation) which was lower than zero ($P<0.001$). There was no significant difference in the mean slopes ($P=0.24$) or the proportion

Table 1 Demographic, clinical and pathologic data of study subjects

Characteristics	N [%]
Total	14 [100]
Sex	
Female	4 [29]
Male	10 [71]
Race/ethnicity	
White and non-Hispanic	14 [100]
Other races/ethnicities	0 [0]
Presence of cardiac disease	4 [29]
Prior chemotherapy	7 [50]
Prior cytoreductive surgery	2 [14]
Pathology	
Biphasic	1 [7]
Epithelioid	13 [93]
Nuclear grade (n=13)	
1	8 [62]
2	4 [31]
3	1 [8]
Cumulative nuclear score (n=13) (nuclear atypia + mitotic counts)	
2	4 [31]
3	4 [31]
4	4 [31]
5	0 [0]
6	1 [8]

of lesions with positive slopes ($P=0.28$) between mass and linear type lesions. The inter- and intra-patient variances were $2.04 \times 10^{-3} \cdot \text{min}^{-2}$ and $0.81 \times 10^{-3} \cdot \text{min}^{-2}$, respectively, yielding an intraclass correlation coefficient of 0.72 [95% confidence interval (CI): 0.56–0.86, $P<0.001$], indicating statistically significant and non-negligible intra-patient correlation.

In per-subject analysis, no statistically significant differences in \tilde{A}_F were found between groups with and without cardiac disease ($P=0.08$), prior chemotherapy ($P=0.62$), or prior cancer reduction surgery ($P=0.44$). Spearman’s coefficients of correlation between \tilde{A}_F and age, nuclear grades, and cumulative nuclear score were -0.33 ($P=0.24$), -0.62 ($P=0.025$), and -0.65 ($P=0.017$; as illustrated

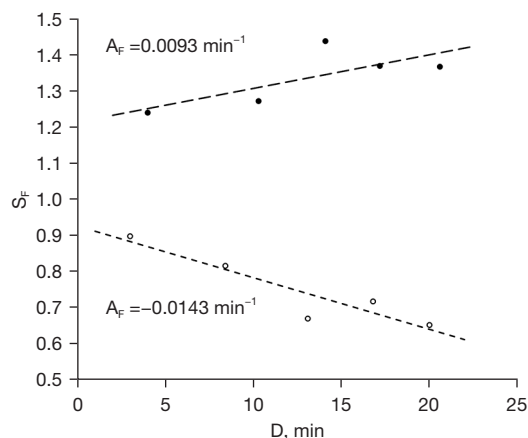


Figure 3 Signal from COR hr T1w mDIXON (in phase) images, normalized to fat (S_F) is plotted against the post-contrast image delay time D , for lesions from two representative subjects, to illustrate the range of A_F . The trendlines (dashed lines) indicate the best linear fit to each lesion’s signal data {see Eq. [1]}. COR hr T1w mDIXON, coronal high-resolution 3D T1-weighted modified Dixon; 3D, three-dimensional.

in Figure 5), respectively.

Qualitative image analysis and correlation to clinical variables

Late delayed images (~19 min post-contrast) were found superior in 55%, equal in 14%, and inferior to the early delayed images (~12 min post-contrast) in 31% of the scans. The cumulative nuclear score was significantly correlated with reader preference ($r=0.65$, $P=0.02$) for reader 1, for both pelvis and right diaphragm. There was no significant correlation when all reader results for both regions were combined ($r=0.27$, $P=0.40$).

Discussion

This phase II clinical trial demonstrates the feasibility of high-resolution, high-contrast MRI of peritoneal mesothelioma with adequate signal-to-noise ratio (SNR), especially in the post-contrast COR hr T1w mDIXON sequence, and describes relation of peritoneal lesion signal intensity with timing of contrast administration.

We introduced several technical advances. First, two high-resolution sequences were implemented. The COR hr T2w SSH FSE sequence was acquired in the respiratory triggered (free breathing, up to two slices per respiratory

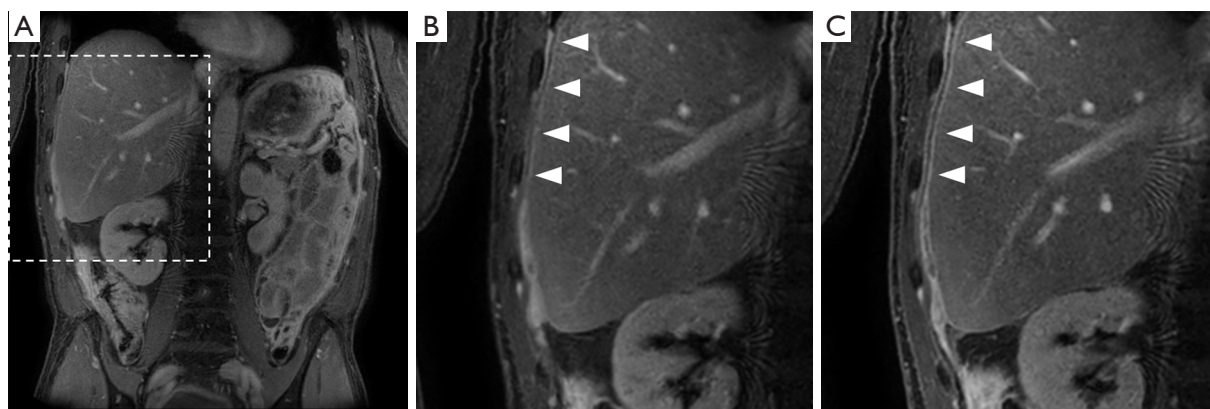


Figure 4 The improved visibility of some lesions in late delayed images is illustrated. (A) A COR hr T1w mDIXON (water-only) image acquired at 9 min delay through the liver of a 67-year-old subject with epithelioid mesothelioma is shown. (B,C) The area outlined in panel A is enlarged to better visualize the lesion (arrowheads), in images taken at 9 min (B) and 19 min delay (C). The lesion conspicuity was clearly increased in the later delayed image (C). COR hr T1w mDIXON, coronal high-resolution 3D T1-weighted modified Dixon; 3D, three-dimensional.

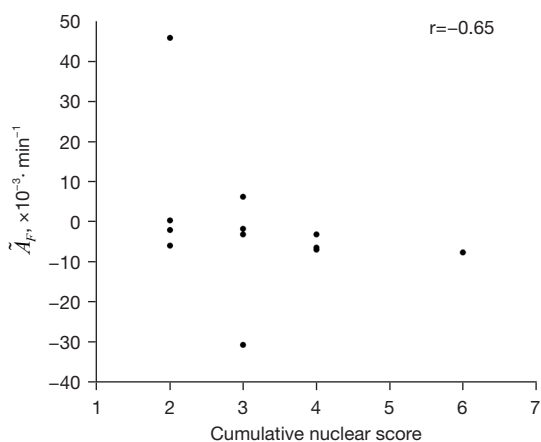


Figure 5 The correlation between the cumulative nuclear score and \tilde{A}_F is illustrated. The Spearman's correlation coefficient is -0.65 ($P=0.017$).

cycle) mode. The spatial resolution was limited by the duration of the respiratory pause after expiration and SNR. The post-contrast COR hr T1w mDIXON images in the abdomen only covered the liver dome in order to maximize the breathhold duration-limited spatial resolution. Second, a double dose of contrast agent was used to enhance lesion visibility. High doses do not produce proportionally higher early peak enhancements due to $T2^*$ effects and non-linearity of T1 shortening effects on signal intensity, but in the delayed post-contrast phases these effects are minimized, improving lesion visibility. Third, we implemented extended

delayed imaging and observed that a large percentage of lesions exhibited persistent enhancement, up to 20 min post-contrast administration, while some were already in the washout phase at 4 min post-contrast.

The COR hr T1w mDIXON acquisition includes multiple breathholds, limiting the achievable temporal resolution. Thus, we were not able to assess the early post-contrast kinetics, but at our delayed imaging times (4+ min), the contrast kinetics is slower and more readily quantifiable. This is in contrast to dynamic contrast-enhanced MRI (DCEMRI) analysis software provided by most MRI manufacturers (23) and to a large number of DCEMRI analysis software packages (24) that use complex pharmacokinetic modeling to quantify contrast agent dynamics but require much higher temporal resolution, especially in the first 1–2 min.

Differences in contrast kinetics point to differences in lesion pathophysiology, which is consistent with our finding that \tilde{A}_F is significantly and strongly correlated to cumulative nuclear score and indicates that a single post-contrast acquisition may not be optimal. Earlier studies have recommended a 5 min post-contrast delay, but longer delays were not evaluated (25–28). A CT study using delays of up to 10 min similarly found 4–5 min to be an optimal delay, but also that many lesions are still enhancing at that time (29). It could be posited that tumors that lead to high fibrotic response that can impede contrast diffusion, or those after neoadjuvant chemotherapy or radiation, might

demonstrate similar delayed contrast enhancement. Our quantitative and qualitative results indicate that acquiring both earlier and later delayed phases could increase the diagnostic accuracy of an MRI exam. Due to similarity of contrast kinetics of CT and most MRI contrast agents, our results could lead to further optimization of the post-contrast imaging timing in peritoneal mesothelioma in both MRI and CT imaging.

Some concerns will need to be addressed before adoption of the proposed MRI protocol in routine clinical practice. Relatively unstably chelated (non-ionic or linear) gadolinium (Gd)-based contrast agents can deposit Gd in tissues, with unclear clinical significance, and care should be taken with administration of double doses (14). This deposition has not been demonstrated with the use of gadoterate meglumine (Dotarem, Guerbet, Paris, France) (16,18). The non-ionic, macrocyclic structure of gadoterate gives it extremely high stability that allows for safe contrast elimination from the body and should be the contrast agent of choice for the proposed protocol (15,17). Further, some institutions may be reluctant to extend the imaging times to 15+ min post-contrast administration. A larger follow up study would provide more information needed to evaluate the diagnostic benefit of the extended delayed imaging and guide this decision.

There are some limitations to this study. First, the low number of participants limited the statistical power. This was due to recruitment from a homogeneous population studied in rigorous clinical trial conditions, with consecutive recruitment used to minimize potential bias. On the other hand, the number of lesions outlined per participant was high, resulting in a high total number of lesions available for analysis. Because the properties of lesions found in the same participant can be correlated, affecting the statistical power, we reported the inter- and intra-subject variability, which can be used to power future studies. Second, while we have demonstrated strong correlation of the contrast enhancement kinetics with cumulative nuclear score, the optimal number and timing of delayed contrast administration is still unclear, as early post-contrast timepoints were not analyzed. Third, the coronal high-resolution T1-weighted sequence did not cover the entire abdomen, but was targeted to areas most likely to contain new lesions, such as the right hemidiaphragmatic recess. Increasing the number of breatholds would allow for expanded anatomical coverage, at the expense of longer acquisition times. Finally, this study was not designed to evaluate the diagnostic performance of the new MRI

protocol. A rigorous comparison of MRI findings with operative findings, to establish diagnostic performance, is underway.

Conclusions

In conclusion, we demonstrated the feasibility of a high-resolution, high-contrast MRI protocol for imaging of peritoneal mesothelioma. High quality post-contrast coronal T1-weighted images demonstrated the necessity of multiple and extended delayed-phase acquisitions due to differences in contrast uptake kinetics in lesions of different nuclear grade. The MRI protocol proposed in this study may allow future imaging adjustments and reduction in management burden and accompanying morbidity for patients with peritoneal mesothelioma.

Acknowledgments

Funding: This work was supported by the Irving Harris Foundation (to K.K.T.), the University of Chicago Comprehensive Cancer Center (to K.K.T.), and the National Institutes of Health (grant Nos. NCATS/NIH UL1 TR000430 and NIH T32CA078586, to K.K.T.).

Footnote

Conflicts of Interest: All authors have completed the ICMJE uniform disclosure form (available at <https://qims.amegroups.com/article/view/10.21037/qims-23-13/coif>). H.L.K. has received consulting fees from AstraZeneca and is on the advisory board of Tempus, Bluestar Genomics, and Sanofi. R.M.E. receives royalties and licensing fees for computer-aided diagnosis technologies through the University of Chicago. A.O. has received funding from NIH and the Sanford J. Grossman Charitable Trust, has received payment for expert testimony, and is a co-owner of Quantitative MR Imaging Solutions (QMIS). S.G.A. is a past president of the International Mesothelioma Interest Group. K.K.T. has received consulting fees from Merck for unrelated work. The other authors have no conflicts of interest to declare.

Ethical Statement: The authors are accountable for all aspects of the work in ensuring that questions related to the accuracy or integrity of any part of the work are appropriately investigated and resolved. The study was conducted in accordance with the Declaration of Helsinki

(as revised in 2013). The study was approved by the Institutional Review Board of the Biological Sciences Division of the University of Chicago (No. IRB18-1011) and informed consent was taken from all individual participants.

Open Access Statement: This is an Open Access article distributed in accordance with the Creative Commons Attribution-NonCommercial-NoDerivs 4.0 International License (CC BY-NC-ND 4.0), which permits the non-commercial replication and distribution of the article with the strict proviso that no changes or edits are made and the original work is properly cited (including links to both the formal publication through the relevant DOI and the license). See: <https://creativecommons.org/licenses/by-nc-nd/4.0/>.

References

1. The Chicago Consensus Guidelines for Peritoneal Surface Malignancies: Introduction. *Ann Surg Oncol* 2020;27:1737-40.
2. Yan TD, Deraco M, Baratti D, Kusamura S, Elias D, Glehen O, Gilly FN, Levine EA, Shen P, Mohamed F, Moran BJ, Morris DL, Chua TC, Piso P, Sugarbaker PH. Cytoreductive surgery and hyperthermic intraperitoneal chemotherapy for malignant peritoneal mesothelioma: multi-institutional experience. *J Clin Oncol* 2009;27:6237-42.
3. Karpes JB, Shamavonian R, Dewhurst S, Cheng E, Wijayawardana R, Ahmadi N, Morris DL. Malignant Peritoneal Mesothelioma: An In-Depth and Up-to-Date Review of Pathogenesis, Diagnosis, Management and Future Directions. *Cancers (Basel)* 2023;15:4704.
4. Steadman JA, Grotz TE. Principles of Surgical Management of Peritoneal Mesothelioma. *J Natl Compr Canc Netw* 2023;21:981-6.
5. Laghi A, Bellini D, Rengo M, Accarpio F, Caruso D, Biacchi D, Di Giorgio A, Sammartino P. Diagnostic performance of computed tomography and magnetic resonance imaging for detecting peritoneal metastases: systematic review and meta-analysis. *Radiol Med* 2017;122:1-15.
6. Sugarbaker PH. Update on the management of malignant peritoneal mesothelioma. *Transl Lung Cancer Res* 2018;7:599-608.
7. Tabrizian P, Jayakrishnan TT, Zacharias A, Aycart S, Johnston FM, Sarpel U, Labow DM, Turaga KK. Incorporation of diagnostic laparoscopy in the management algorithm for patients with peritoneal metastases: A multi-institutional analysis. *J Surg Oncol* 2015;111:1035-40.
8. Low RN, Barone RM. Imaging for Peritoneal Metastases. *Surg Oncol Clin N Am* 2018;27:425-42.
9. Low RN, Barone RM, Duggan B, Bahador A, Daniels C, Veerapong J. Detection of Mesenteric Tumor Using Dynamic Contrast Enhanced MRI. *Ann Surg Oncol* 2020;27:2525-36.
10. Kusamura S, Kepenekian V, Villeneuve L, Lurvink RJ, Govaerts K, De Hingh IHJT, Moran BJ, Van der Speeten K, Deraco M, Glehen O; SOGI. Peritoneal mesothelioma: SOGI/EURACAN clinical practice guidelines for diagnosis, treatment and follow-up. *Eur J Surg Oncol* 2021;47:36-59.
11. Low RN, Barone RM, Rousset P. Peritoneal MRI in patients undergoing cytoreductive surgery and HIPEC: History, clinical applications, and implementation. *Eur J Surg Oncol* 2021;47:65-74.
12. Yamamuro M, Gerbaudo VH, Gill RR, Jacobson FL, Sugarbaker DJ, Hatabu H. Morphologic and functional imaging of malignant pleural mesothelioma. *Eur J Radiol* 2007;64:356-66.
13. Chapel DB, Schulte JJ, Absenger G, Attanoos R, Brcic L, Butnor KJ, Chiriac L, Churg A, Galateau-Sallé F, Hiroshima K, Hung YP, Kindler H, Krausz T, Marchevsky A, Mino-Kenudson M, Mueller J, Nabeshima K, Turaga K, Walts AE, Husain AN. Malignant peritoneal mesothelioma: prognostic significance of clinical and pathologic parameters and validation of a nuclear-grading system in a multi-institutional series of 225 cases. *Mod Pathol* 2021;34:380-95.
14. Fraum TJ, Ludwig DR, Bashir MR, Fowler KJ. Gadolinium-based contrast agents: A comprehensive risk assessment. *J Magn Reson Imaging* 2017;46:338-53.
15. Morcos SK. Extracellular gadolinium contrast agents: differences in stability. *Eur J Radiol* 2008;66:175-9.
16. Lersy F, Diepenbroek AL, Lamy J, Willaume T, Bierry G, Cotton F, Kremer S. Signal changes in enhanced T1-weighted images related to gadolinium retention: A three-time-point imaging study. *J Neuroradiol* 2021;48:82-7.
17. Frenzel T, Lengsfeld P, Schirmer H, Hütter J, Weinmann HJ. Stability of gadolinium-based magnetic resonance imaging contrast agents in human serum at 37 degrees C. *Invest Radiol* 2008;43:817-28.
18. Perrotta G, Metens T, Absil J, Lemort M, Manto M. Absence of clinical cerebellar syndrome after serial injections of more than 20 doses of gadoterate, a

- macrocyclic GBCA: a monocenter retrospective study. *J Neurol* 2017;264:2277-83.
19. Mahmood F, Nielsen UG, Jørgensen CB, Brink C, Thomsen HS, Hansen RH. Safety of gadolinium based contrast agents in magnetic resonance imaging-guided radio-therapy - An investigation of chelate stability using relaxometry. *Phys Imaging Ra-diat Oncol* 2022;21:96-100.
 20. Harris PA, Taylor R, Minor BL, Elliott V, Fernandez M, O'Neal L, McLeod L, De-lacqua G, Delacqua F, Kirby J, Duda SN; REDCap Consortium. The REDCap consortium: Building an international community of software platform partners. *J Bi-omed Inform* 2019;95:103208.
 21. Harris PA, Taylor R, Thielke R, Payne J, Gonzalez N, Conde JG. Research electronic data capture (REDCap)-a metadata-driven methodology and workflow process for providing translational research informatics support. *J Biomed Inform* 2009;42:377-81.
 22. Kadota K, Suzuki K, Colovos C, Sima CS, Rusch VW, Travis WD, Adusumilli PS. A nuclear grading system is a strong predictor of survival in epitheloid diffuse malignant pleural mesothelioma. *Mod Pathol* 2012;25:260-71.
 23. Beuzit L, Eliat PA, Brun V, Ferré JC, Gandon Y, Bannier E, Saint-Jalmes H. Dy-namic contrast-enhanced MRI: Study of inter-software accuracy and reproducibility using simulated and clinical data. *J Magn Reson Imaging* 2016;43:1288-300.
 24. Barnes SR, Ng TS, Santa-Maria N, Montagne A, Zlokovich BV, Jacobs RE. ROCK-ETSHIP: a flexible and modular software tool for the planning, processing and analysis of dynamic MRI studies. *BMC Med Imaging* 2015;15:19.
 25. Elsayes KM, Staveteig PT, Narra VR, Leyendecker JR, Lewis JS Jr, Brown JJ. MRI of the peritoneum: spectrum of abnormalities. *AJR Am J Roentgenol* 2006;186:1368-79.
 26. Low RN. Gadolinium-enhanced MR imaging of liver capsule and peritoneum. *Magn Reson Imaging Clin N Am* 2001;9:803-19, vii.
 27. Low RN. Preoperative and surveillance MR imaging of patients undergoing cy-toreductive surgery and heated intraperitoneal chemotherapy. *J Gastrointest Oncol* 2016;7:58-71.
 28. Patel AM, Berger I, Wileyto EP, Khalid U, Torigian DA, Nachiappan AC, Barbosa EM Jr, Gefter WB, Galperin-Aizenberg M, Gupta NK, Simone CB 2nd, Haas AR, Alley EW, Singhal S, Cengel KA, Katz SI. The value of delayed phase enhanced imaging in malignant pleural mesothelioma. *J Thorac Dis* 2017;9:2344-9.
 29. Patel A, Roshkovan L, McNulty S, Alley E, Torigian DA, Nachiappan AC, Galperin-Aizenberg M, Barbosa EM Jr, DiRienzi J, Berger I, Khalid U, Haas AR, Singhal S, Wileyto EP, Cengel KA, Katz SI. Delayed-Phase Enhancement for Eval-uation of Malignant Pleural Mesothelioma on Computed Tomography: A Prospective Cohort Study. *Clin Lung Cancer* 2021;22:210-217.e1.

Cite this article as: Medved M, Witmer HDD, Dhiman A, Berger Y, Sherman SK, Hindi ES, Armato SG 3rd, Reiser IS, Oto A, Engelmann RM, Kindler HL, Oren NC, Harmath CB, Turaga KK. Im-plementation of a high resolution, high-contrast magnetic resonance imaging protocol with extended delayed phases for peritoneal mesothelioma. *Quant Imaging Med Surg* 2024;14(3):2580-2589. doi: 10.21037/qims-23-13

Table S1 MRI protocol and sequence parameters

Name	Sequence type	TR/TE (ms)	Flip angle (°)	FS	FOV (mm ²)	Resolution (ACQ) (mm ³)	Slice gap (mm)	Resolution (REC) (mm ³)	SENSE	Duration (min:second)	Post-contrast delay (min)
AX T2w ABD + PEL BH	2D SSH FSE	1,250/80	90	–	430×300×485	1.3×1.5×5	0.5	0.81×0.81×5	1.75 AP	1:50	–
AX T2w FS ABD + PEL RT	2D mSH FSE	2,350/80	90	SPIR	430×300×485	1.2×1.4×5	0.5	0.81×0.81×5	1.3 AP	4:12	–
COR T2w ABD + PEL BH	2D SSH FSE	1,250/80	90	–	285×430×470	1.4×1.6×5	0.5	0.45×0.45×5	2.5 RL	1:50	–
COR hr T2w ABD + PEL RT [†]	2D SSH FSE	2,000/80	90	–	285×430×455	0.80×0.80×3	0	0.61×0.61×3	3.2 RL	7:30	–
COR PRE hr T1w ABD mDIXON BH [‡]	3D FFE mDIXON	4.0/1.4, 2.6	10	Post-processing	400×430×190	1.2×1.16×3	–	0.89×0.89×1.5	2.2 RL, 1.7 AP	0:45	–
AX PRE T1w PEL mDIXON BH	3D FFE mDIXON	3.6/1.32, 2.3	10	Post-processing	430×300×270	1.60×1.7×3.5	–	0.9×0.9×1.75	2.0 AP, 1.5 FH	0:18	–
AX PRE T1w ABD mDIXON BH	3D FFE mDIXON	3.6/1.32, 2.3	10	Post-processing	430×300×270	1.60×1.7×3.5	–	0.9×0.9×1.75	2.0 AP, 1.5 FH	0:18	–
Administration of 0.2 mmol/kg of gadoterate meglumine [‡]											
COR POST hr T1w ABD mDIXON BH [†]	3D FFE mDIXON	4.0/1.4, 2.6	10	Post-processing	400×430×190	1.2×1.16×3	–	0.89×0.89×1.5	2.2 RL, 1.7 AP	0:45	4, 7
AX POST T1w ABD mDIXON BH	3D FFE mDIXON	3.6/1.32, 2.3	10	Post-processing	430×300×270	1.60×1.7×3.5	–	0.9×0.9×1.75	2.0 AP, 1.5 FH	0:18	10
AX POST T1w PEL mDIXON BH	3D FFE mDIXON	3.6/1.32, 2.3	10	Post-processing	430×300×270	1.60×1.7×3.5	–	0.9×0.9×1.75	2.0 AP, 1.5 FH	0:18	11
COR POST hr T1w ABD mDIXON BH [†]	3D FFE mDIXON	4.0/1.4, 2.6	10	Post-processing	400×430×190	1.2×1.16×3	–	0.89×0.89×1.5	2.2 RL, 1.7 AP	0:45	13, 16, 20
COR POST hr T1w PEL mDIXON BH [†]	3D FFE mDIXON	4.0/1.4, 2.6	10	Post-processing	400×430×190	1.2×1.16×3	–	0.89×0.89×1.5	2.2 RL, 1.7 AP	0:45	23

[†], research high-resolution sequence; [‡], double dose of gadoterate meglumine (Dotarem, Guerbet LLC, Princeton, NJ, USA). Total scan time listed: ~20 min. Total exam duration: ~60 min (includes survey sequences, prescan times, and breathhold recovery). MRI, magnetic resonance imaging; TR, repetition time; TE, echo time; FS, fat suppression; FOV, field of view; ACQ, as acquired; REC, as reconstructed; SENSE, sensitivity encoding; AX, axial orientation; T2w, T2-weighted; ABD + PEL, ABD and PEL were acquired in two stages; ABD, abdominal; PEL, pelvic; BH, breath-hold; 2D, two-dimensional; SSH FSE, single-shot fast spin echo; AP, anterior/posterior direction; RT, respiratory triggered; mSH FSE, multi-shot fast spin echo; SPIR, spectral presaturation with inversion recovery; COR, coronal orientation; RL, right/left direction; hr, high-resolution; PRE, pre-contrast administration; T1w, T1-weighted; mDIXON, modified Dixon; 3D, three-dimensional; FFE, fast field echo; FH, foot/head direction; POST, post-contrast administration.